Hole conductivity through a defect band in $ZnGa_2O_4$

Fernando P. Sabino [1], Intuon Chatratin,[2] Anderson Janotti,[2] and Gustavo M. Dalpian [1]

[1]*Centro de Ciências Naturais e Humanas, Universidade Federal do ABC, 09210-580 Santo André, São Paulo, Brazil*
[2]*Department of Materials Science and Engineering, University of Delaware, Newark, Delaware 19716, USA*

Semiconductors with a wide band gap (>3.0 eV), high dielectric constant (>10), good thermal dissipation, and capable of n- and p-type doping are highly desirable for high-energy power electronic devices. Recent studies indicate that $ZnGa_2O_4$ may be suitable for these applications, standing out as an alternative to Ga_2O_3. The simple face-centered-cubic spinel structure of $ZnGa_2O_4$ results in isotropic electronic and optical properties, in contrast to the large anisotropic properties of the β-monoclinic Ga_2O_3. In addition, $ZnGa_2O_4$ has shown, on average, better thermal dissipation and potential for n- and p-type conductivity. Here we use density functional theory and hybrid functional calculations to investigate the electronic, optical, and point defect properties of $ZnGa_2O_4$, focusing on the possibility for p- and n-type conductivity. We find that the cation antisite Ga_{Zn} is the lowest-energy donor defect that can lead to unintentional n-type conductivity. The stability of self-trapped holes (small hole polarons) and the high formation energy of acceptor defects make it difficult to achieve p-type conductivity. However, with an excess of Zn, forming $Zn_{(1+2x)}Ga_{2(1-x)}O_4$ alloys, this compound can display an intermediate valence band, facilitating p-type conductivity. Due to the localized nature of this intermediate valence band, p-type conductivity by polaron hopping is expected, explaining the low mobility and low hole density observed in recent experiments.

I. INTRODUCTION

Ultrawide band-gap semiconductors have attracted great attention in recent years for their application in high-power transistors for energy conversion and solar-blind ultraviolet (UV) detectors, combining high critical electric field strength, transparency in the visible spectrum, and high conductivity through doping [1–5]. Among the promising semiconductor materials, Ga_2O_3 stands out with a band gap in the range of 4.6–5.0 eV and a large electric breakdown field, resulting in Baliga's figure of merit just smaller than diamond and with capability that goes beyond existent technologies based on SiC and GaN [1,6]. However, the low thermal conductivity and the complicated monoclinic crystal structure of β-Ga_2O_3 lead to low heat dissipation and anisotropic electronic and optical properties, which, in addition to the inherent difficulties in making the material p-type or even reliably semi-insulating, pose serious obstacles to device design and implementation [2,3,6,7].

Recent studies have focused on $ZnGa_2O_4$ as a ultrawide band-gap semiconductor for devices [2–5]. With a band gap of 5.0 eV, room-temperature electron mobility of 10^2 cm^2/V s, and high dielectric constant of 10.4, $ZnGa_2O_4$ has been considered as an alternative or, at least, as a complement to Ga_2O_3 [3–5]. Thin films of spinel $ZnGa_2O_4$ have been grown epitaxially on sapphire substrate [5]. As this material crystallizes in the cubic phase, the optical and electronic properties are isotropic. Considering an average in all directions, experimental results indicate that the thermal dissipation in $ZnGa_2O_4$ thin films is about 10% more efficient than in Ga_2O_3 [3,8].

Reported unintentional n-type conductivity in $ZnGa_2O_4$ with carrier density of 9×10^{19} cm^{-3} is three orders of magnitude higher than that in undoped Ga_2O_3 and one order of magnitude higher than in Si- or Sn-doped Ga_2O_3 [4–6,9]. The possible source of this unintentional n-type doping in $ZnGa_2O_4$ is still under debate, being attributed to oxygen vacancies (V_O), antisites such as Ga on Zn site (Ga_{Zn}), or a combination of both [4,5]. The oxygen vacancy was predicted to be a shallow donor in some oxides, such as In_2O_3, for example [10]. However, in oxides with wider band gaps, such as Ga_2O_3 or ZnO, the oxygen vacancy was predicted to behave as a deep donor and could not contribute to the observed unintentional n-type conductivity [11,12]. Similarly, it is expected that the unintentional conductivity observed in $ZnGa_2O_4$ cannot be explained by the presence of V_O.

Recent experimental results also indicate that $ZnGa_2O_4$ shows p-type conductivity when grown in an O-rich flux condition [4,5], with hole concentrations reaching 10^{15} cm^{-3} at 800 K [4], and an extracted activation energy of 0.93 eV. Such high thermal activation energy was attributed to intraband conduction according to Chikoidze *et al.* [4]. This is an intriguing result considering the very low valence-band maximum (high work function) of $ZnGa_2O_4$. If both p- and n-type conductivity could be achieved in the wide band gap $ZnGa_2O_4$, this material would become a potential candidate for a solid-state deep UV light emitting diode (LED), with photon energies in the window of 254–207 nm that is appropriate for eliminating virus and bacterias, including SARS-COV 19 [13].

Although $ZnGa_2O_4$ is already being used as a transparent conducting oxide, the role of native point defects in

their electronic and optical properties is still a subject of debate and not widely explored in the literature [14–16]. Using calculations based on density functional theory (DFT) and hybrid functionals, we calculate the formation energies and transition levels for native point defects in $ZnGa_2O_4$. We find that the Ga_{Zn} antisite is a shallow donor and likely the main source of unintentional *n*-type conductivity in $ZnGa_2O_4$. On the other hand, none of the native point defects are shallow acceptors and can lead to *p*-type conductivity. Moreover, holes tend to become self-trapped, forming small polarons.

On the other hand, if an excess of Zn is incorporated in $ZnGa_2O_4$, forming $Zn_{(1+2x)}Ga_{2(1-x)}O_4$ alloys, the extra Zn occupying the Ga sites leads to a partially occupied intermediate valence band, within which holes existing as small polarons move by hopping, possibly explaining the observed *p*-type conductivity [4,5]. We also construct configuration coordinate diagrams to determine the energy of the optical emission peaks associated with each defect to help their identification, with special attention to the oxygen vacancy, the self-trapped hole, and the Ga_{Zn} antisite.

II. THEORETICAL APPROACH AND COMPUTATIONAL DETAILS

Our calculations are based on density functional theory (DFT) [17,18] and the Heyd-Scuseria-Ernzerhof (HSE) hybrid functional [19,20] as implemented in the Vienna Ab Initio Simulation Package (VASP) [21,22]. The interaction between the valence electrons and the ionic cores was treated using projected augmented wave (PAW) potentials [23,24], considering the following valence configurations: $O(2s^2 2p^4)$, $Ga(3d^{10}4s^2 4p^1)$, and $Zn(3d^{10}4s^2)$. In the HSE functional, the exchange is separated in two regions, long and short range, by a screening parameter $\omega = 0.20$ [19,20]. In the default configuration, the short-range region is composed of 25% of nonlocal Hartree-Fock exchange, and the remaining 75% derives from the Perdew-Burke-Ernzerhof (PBE) functional. All of the correlation and exchange for the long-range region are derived from the PBE functional [19,20]. However, the default value for the amount of Hartree-Fock exchange is not enough to correct the band gap for both Ga_2O_3 and ZnO, and we expect the same behavior for $ZnGa_2O_4$. Here we find that a mixing parameter of 33% is necessary to give a band gap of 4.9 eV for $ZnGa_2O_4$, which leads to a good agreement with recent experimental data [4,5].

The stress tensor and the atomic forces were minimized for the primitive spinel structure of $ZnGa_2O_4$ within the HSE functional using a plane-wave cutoff energy of 600 eV. For the Brillouin zone integration, we employed a **k** mesh of $5 \times 5 \times 5$, and for the density of states (DOS), we increased the mesh to $9 \times 9 \times 9$. The formation energies of defects and the emission spectrum were computed using a supercell that is a $2 \times 2 \times 2$ repetition of the primitive spinel, totaling a structure with 112 atoms. We have used the low-symmetry special **k** point $(1/4, 1/4, 1/4)$ in all supercell calculations [25]. To obtain this size of cell, we performed a convergence test as a function of the cell size, which is shown in Fig. S6 in the Supplemental Material [26].
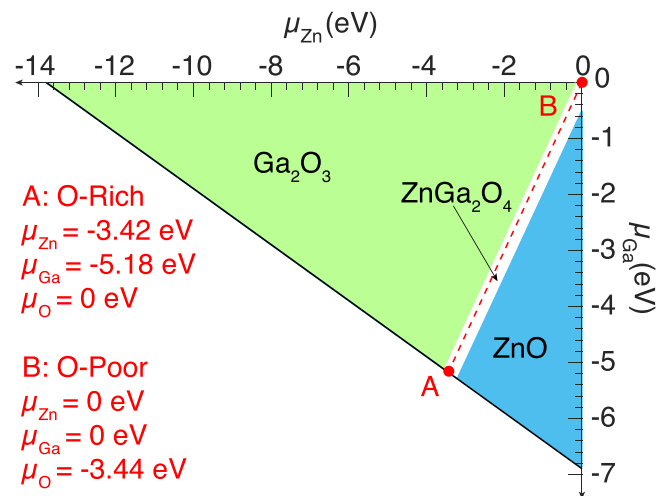

FIG. 1. Phase diagram (or stability triangle) for $ZnGa_2O_4$. The white area represents the chemical potentials that lead $ZnGa_2O_4$ with higher stability when compared to the unary oxides of ZnO and Ga_2O_3. Points A and B represent the condition of O rich and O poor, respectively, and the chemical potentials for O, Zn, and Ga are shown for both points.

Defect formation energies

The formation energy of a defect D in the charge state q was calculated according to the following expression:

$$E^f(D, q) = E_{tot}(D, q) - E_{tot}^B + \sum_i n_i \mu_i + qE_F + \Delta^q, \quad (1)$$

where $E_{tot}(D, q)$ is the total energy of the supercell containing a defect D in charge state q, and E_{tot}^B is the total energy of perfect bulk $ZnGa_2O_4$ in the same supercell. The chemical potential μ_i for the specie i that was removed or added to the supercell for the defect is referenced to the total energy of the respective elemental phase. E_F is the parametric Fermi energy taking the valence-band maximum (VBM) as a reference, and Δ^q is the charge-state-dependent correction due to the finite size of the supercell [27,28].

The chemical potentials are treated as variables in Eq. (1). To ensure the stability of $ZnGa_2O_4$, the chemical potentials should satisfy the following condition:

$$\mu_{Zn} + 2\mu_{Ga} + 4\mu_O = \Delta H_f(ZnGa_2O_4), \quad (2)$$

where $\Delta H_f(ZnGa_2O_4)$ is the formation enthalpy of $ZnGa_2O_4$; we find $\Delta H_f(ZnGa_2O_4) = -13.79$ eV using HSE. To avoid the formation of competing phases, such as Ga_2O_3 and ZnO, the chemical potentials must also satisfy

$$2\mu_{Ga} + 3\mu_O < \Delta H_f(Ga_2O_3), \quad \mu_{Zn} + \mu_O < \Delta H_f(ZnO), \quad (3)$$

where $\Delta H_f(Ga_2O_3)$ and $\Delta H_f(ZnO)$ are the formation enthalpies of β-Ga_2O_3 and wurtzite ZnO. Following these relations, we can determine the region of stability for $ZnGa_2O_4$ in the phase diagram as shown in Fig. 1. The blue and green areas show the regions where the oxides ZnO and Ga_2O_3 are stable, while the white area represents the region where $ZnGa_2O_4$ is stable. In the phase diagram, we choose two points, A and B, for which the defect formation energies
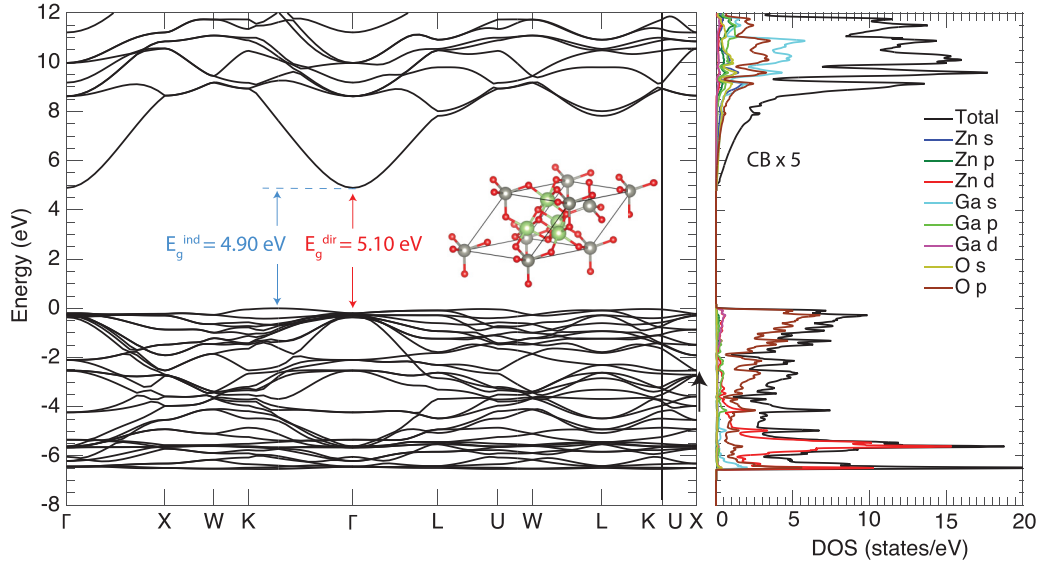
FIG. 2. Band structure and density of states for the fcc spinel structure of $ZnGa_2O_4$ taking the VBM as a reference. The band gap is indirect with the VBM located along the Γ-K direction, and the CBM occurs at Γ. Inset: The crystal structure of $ZnGa_2O_4$, where Zn, Ga, and O are shown by the gray, green, and red spheres, respectively.

are reported, representing O-rich and O-poor limit conditions, respectively.

To compute the energy of the light absorption and emission peaks associated with point defects, we use the Franck-Condon principle through the construction of generalized coordinate diagrams [29,30]. It is assumed that for a given defect, the optical transition from the defect in charge state q to a charge state $q + 1$ (or $q - 1$) is so fast that the lattice around the defect does not have time to relax. So the optical transition level from a charge state q to the charge state $q + 1$ is given by the formation energy difference between the defect in charge state q and charge state $q + 1$, both in the lattice configuration corresponding to that of the initial charge state q [10,29–31]. We also performed a convergence test for the emission spectrum as a function of the cell size; the results are shown in Fig. S6 in the Supplemental Material [26].

III. RESULTS AND DISCUSSION

A. Crystal structure and electronic properties

$ZnGa_2O_4$ crystallizes in the face-centered-cubic (fcc) spinel structure that belongs to the $Fm\bar{3}m$ space group with an experimental equilibrium lattice parameter of $a_0 = 8.33$ Å [4] (the crystal structure is shown in the inset of Fig. 2). The calculated equilibrium lattice parameter of 8.36 Å is only 0.36% larger than the experimental value. In the spinel crystal structure, the oxygen atoms occupy a unique nonequivalent site with Wyckoff notation $32e$, where each O is bound to four cations (three Ga and one Zn). On the other hand, there are two nonequivalent cation sites, with completely different chemical environments. One of these sites is surrounded by six oxygen atoms, forming perfect octahedral motifs ($16d$ in the Wyckoff notation) and occupied by Ga atoms, while the second site forms a perfect tetrahedral chemical environment ($8a$ in the Wyckoff notation) occupied by Zn atoms. All the

local chemical environments are shown in Fig. S1 in the Supplemental Material [26].

The electronic band structure and density of states of $ZnGa_2O_4$, calculated using HSE, are shown in Fig. 2. The valence band is mainly derived from O $2p$ orbitals, with the VBM located in between the K and Γ points; it shows low dispersion (high effective masses) and we expect a high ionization potential (not shown in Fig. 2) due to the orbital character composition. In contrast, the conduction band is composed mainly of Zn and Ga s orbitals, resulting in a large dispersion conduction-band minimum (CBM), with a minimum at Γ. The calculated indirect band gap is 4.90 eV. The local maximum in the valence band at Γ lies only 0.20 eV below the VBM, leading to a direct band gap of 5.10 eV. The indirect band-gap nature of the $ZnGa_2O_4$ spinel was reported by previous works using DFT with Hubbard-U correction (DFT+U) [14,15].

The dispersion of the VBM in $ZnGa_2O_4$ is affected by the p-d coupling. In ZnO, the coupling between the Zn d and O p orbitals shifts the position of the VBM to higher energies, increasing the dispersion in the vicinity of the VBM [11]. The position of Ga d orbitals in Ga_2O_3, on the other hand, is significantly lower than the VBM, resulting in a weaker p-d coupling and a low dispersion of the VBM [32,33]. In $ZnGa_2O_4$, the p-d coupling has an intermediate intensity, lying between the cases of ZnO and Ga_2O_3, with contributions from both cation's d orbitals. Zn d orbitals are located around 4 eV below the VBM, as indicated by the red line in the orbital-resolved DOS in Fig. 2, while Ga $3d$ orbitals lie 14 eV below the VBM (not shown in Fig. 2). Despite the moderated p-d coupling, the intensity is not sufficient to increase the dispersion of the VBM in $ZnGa_2O_4$.

B. Intrinsic defects

We investigate all the possible intrinsic point defects in $ZnGa_2O_4$, i.e., vacancies (V_O, V_{Zn} and V_{Ga}), antisites (Ga_{Zn},
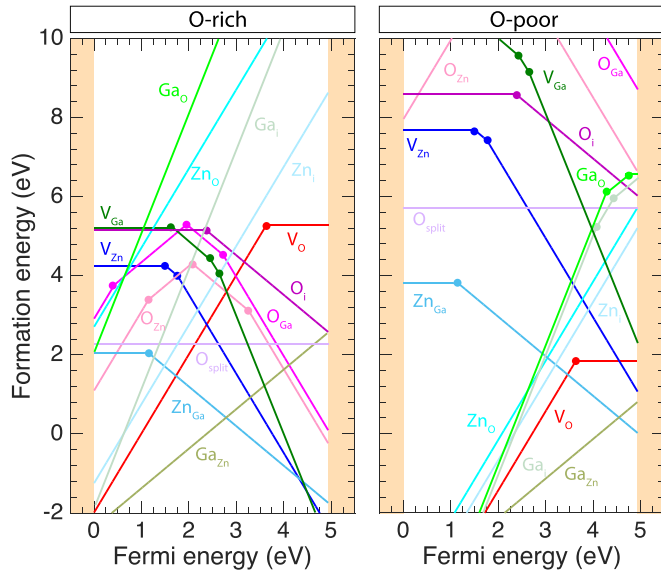
FIG. 3. Formation energy as a function of the parametric Fermi energy for all intrinsic defects in $ZnGa_2O_4$ calculated in O-rich and -poor chemical potentials, which are represented in Fig. 1. The defects that are associated with oxygen are represented in red tons, the ones associated with zinc in blue, and the ones for Ga in green.

Ga_O, Zn_{Ga}, Zn_O, O_{Zn} and O_{Ga}), and interstitials (Zn_i, Ga_i and O_i), as well as the self-trapped hole in the form of a small hole polaron. The defect formation energies as a function of Fermi level for O-rich (point A) and O-poor (point B) conditions are shown in Fig. 3.

The equilibrium Fermi level, which is not the same as the parametric Fermi level, lies close to the crossing point of the donor and acceptor defects with the lowest formation energy in Fig. 3, i.e., near the crossing of Ga_{Zn}^{1+} and Zn_{Ga}^{1-}. For O rich (poor), $E_F^{eq} = 2.78$ eV ($E_F^{eq} = 4.58$ eV). However, in the discussion below, we consider an analysis based on the parametric Fermi level. This idea is associated with a possible variation of this equilibrium Fermi level, which can occur owing to extrinsic dopant, passivation of native defects, or other external conditions.

For the Fermi level near the valence band and for the O-rich condition, the most stable defects are Ga_{Zn}, Ga_i, Zn_i, and V_O; they are all donor defects. In contrast, for the Fermi level near the conduction band, V_{Zn}, V_{Ga}, and Zn_{Ga} are the lowest-energy defects and act as acceptors. For the O-poor condition, the results are similar; however, the donors Ga_O and Zn_O are also low formation energy defects for the Fermi level below the middle of the band gap.

It is important to mention that in O-rich conditions, the acceptor defects are predominant in the region close to the CBM. The formation energy of these acceptor defects is significantly lower than any donor defect and, therefore, we expect n-type conductivity under the O-rich condition to be very difficult to achieve due to compensation. On the other hand, acceptor defects are high formation energy defects in the region near the VBM for the O-poor condition, preventing, in principle, p-type conductivity. We also note that the lowest-energy defect that can cause n-type (p-type) conductivity is Ga_{Zn} (Zn_{Ga}), i.e., the cation antisites. This explains the observation of Ga

(Zn) occupying the tetrahedral (octahedral) site in the spinel structure [3–5]. The most likely source of unintentional n-type conductivity in $ZnGa_2O_4$ is Ga_{Zn}, whereas V_O, often pointed to as the source of unintentional n-type conductivity in many oxides, is a deep donor. In the following, we discuss the details of each defect in $ZnGa_2O_4$, separating the discussion on hole polaron, vacancies, antisites, and interstitial defects.

1. Small hole polaron

We find that a hole in the valence band of $ZnGa_2O_4$ spontaneously becomes self-trapped, forming a small hole polaron, as predicted for other oxides and in agreement with previous works in $ZnGa_2O_4$ [16,34,35]. It is localized on one oxygen atom and accompanied by a local lattice distortion where one O-Ga bond length increased by 23%, transforming the tetrahedral environment around O to an almost trigonal planar configuration, with the wave function resembling that of an O $2p_z$ orbital, as shown in Fig. 4(a). This effect is caused by the rather low dispersion and low energy of the valence band in $ZnGa_2O_4$. The calculated hole self-trapping energy of 0.44 eV is basically defined as the difference between the total energy of the supercell containing one localized hole (by removing an electron from the supercell and letting the atomic positions relax) and the supercell with a hole at the VBM [34]. We expect that the energy gained from a self-trapped hole in $ZnGa_2O_4$ is similar to that in Ga_2O_3, with a relatively large increase in the Ga-O bond lengths and a small variation of the Zn-O bond. In fact, our result of 0.44 eV for the hole self-trapping energy in $ZnGa_2O_4$ is similar to the 0.53 eV previously reported in Ga_2O_3 [34,35], but 0.23 eV larger than recently published work for $ZnGa_2O_4$ [16]. The relatively large self-trapping energy (much higher than k_BT at room temperature) in $ZnGa_2O_4$ indicates that hole conductivity, if realized, will be through small polaron hopping, with characteristic low mobility at room temperature.

2. Vacancies

Oxygen vacancy. When an oxygen vacancy is created in $ZnGa_2O_4$, four bonds are broken (three with Ga and one with Zn), leaving four dangling bonds. This electronic configuration reorganizes in low-energy nondegenerate and high-energy threefold degenerate single-particle states. In the neutral charge state, the lower onefold degenerate state is occupied with two electrons and located in the band gap, 2.47 eV above the VBM, while the threefold state is unoccupied and lies resonant in the conduction band. Under this charge state, the atoms in the vicinity of V_O relax inward by 14.51% of the equilibrium Zn-O bond length and the Ga atoms relax inward by 0.50% of the equilibrium Ga-O bond length, as indicated in Fig. 4(b). Removing one electron from the gap state leads to a 1+ charge state, V_O^{1+}; the gap state splits into spin-up occupied and spin-down unoccupied states, located at 2.90 and 4.53 eV above the VBM, respectively. The neighboring Zn atoms relax outward from the vacancy by 6.21% and Ga by 5.90% of the respective equilibrium bond length. In the 2+ charge state, the lower state is also completely unoccupied and is shifted up to inside the conduction band. Under this charge state, the neighboring atoms further relax outward: the Zn by 30.05% and the three Ga 11.38%, as shown in Fig. 4(c).
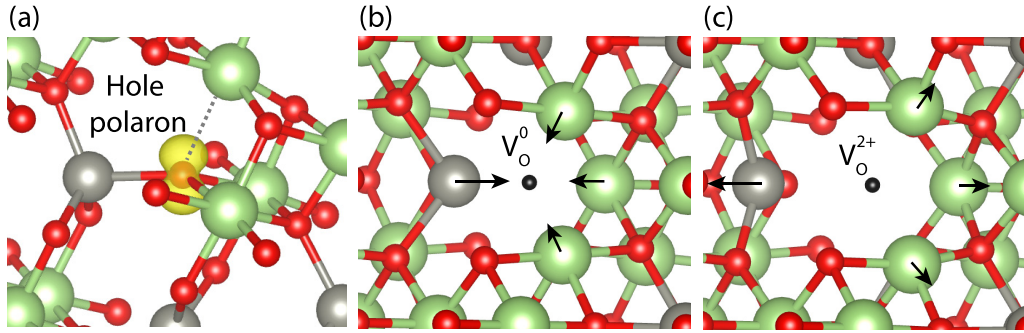
FIG. 4. Local atomic environment representing the (a) hole polaron, with the local charge density (yellow); (b) oxygen vacancy in the neutral charge state, V_O^0; and (c) oxygen vacancy in the 2+ charge state, V_O^{2+}. The arrows indicate the local lattice relaxations with respect to the system without defects. The oxygen, zinc, and gallium atoms are represented by the red, gray, and green colors, respectively.

The neighboring Zn atom around the V_O^{2+} forms an almost trigonal planar motif.

The formation energies as a function of the Fermi level (E_F) for V_O in different charge states are shown in Fig. 3. We observe that V_O^{1+} is not stable for all possible values of E_F when compared to the neutral and 2+ charge states. This indicates that the gap state is either fully occupied with two electrons or an empty resonant in the conduction band. The thermodynamic transition level from a neutral to 2+ charge state occurs at 1.26 eV below the CBM, making V_O a deep donor and unlikely to contribute to n-type conductivity when E_F is close to the CBM and at room temperature. On the other hand, if the Fermi level lies in the middle of the band gap (insulator) or close to the VBM (p-type), V_O acts as a compensation defect for holes. The low or negative formation energy of V_O in an O-poor condition, second lower among all the intrinsic donor defects, makes it very difficult to result in ZnGa$_2$O$_4$ p-type. The deep donor behavior of V_O was also reported in a previous DFT+U work [15].

Therefore, in addition to the high stability of the hole polaron discussed before, this is another problem to realize p-type conductivity in ZnGa$_2$O$_4$. In contrast, V_O also does not act as a source of free electrons when the Fermi level in ZnGa$_2$O$_4$ is close to the CBM and the n-type conductivity is predominant. This behavior is different when compared to In$_2$O$_3$ [10], but similar to ZnO [11] and Ga$_2$O$_3$ [12].

Zinc vacancy. The removal of a Zn atom results in two holes in the valence band that tend to localize in the form of small hole polarons at the O $2p_z$ orbital of two different O atoms neighboring the vacancy (V_{Zn}^0); these small polarons are associated with unoccupied single-particle states in the gap, in opposite spin channels.

By adding one electron to V_{Zn}^0, one of the small hole polarons vanishes, resulting in the negatively charged state V_{Zn}^{1-}, with a $(0/-)$ transition level at 1.51 eV above the VBM. Introducing a second electron fills the remaining single-particle level of V_{Zn}^{1-} inside the band gap, resulting in V_{Zn}^{2-}. The $(-/2-)$ transition level is at 1.76 eV above the VBM. The local lattice configuration around V_{Zn}^{2-} is shown in Fig. S2 in the Supplemental Material [26].

The formation energy of V_{Zn} is low and even becomes negative in O-rich conditions when E_F is near the CBM. This indicates that V_{Zn} is a likely source of electron compensation in n-type ZnGa$_2$O$_4$. For E_F near the VBM, V_{Zn} has high formation energy. The position of the $(0/-)$ and $(-/2-)$ transition levels well above the VBM indicates that V_{Zn} is a deep acceptor and cannot serve as a source of p-type conductivity.

Gallium vacancy. The vacancy of Ga is similar to Zn. Because of the 3+ oxidation state of Ga, three holes are generated in the system when a V_{Ga} is created. These three holes tend to localize in the form of small polarons and sit on three different O $2p_z$ orbitals around the V_{Ga}, maximizing the distance between them. When an electron is added to the system, one empty quasiparticle state that lies in the band gap (neutral charge state) become completely occupied and moves toward the valence band. This condition represents the V_{Ga}^{1-} charge state and the transition from $(0/-)$ occur at 1.63 eV above the VBM. Similar behavior is observed for the other negative charge states, with transitions $(-/2-)$ and $(2-/3-)$ lying at 2.40 and 2.53 eV above the VBM. All these transitions can be observed in the formation energy of Fig. 3 and the atomic configuration for V_{Ga}^{3-} is shown in Fig. S2 in the Supplemental Material [26].

In the O-rich limit condition, the formation energy of V_{Ga} becomes low or negative for E_F in the upper part of the band gap, while in the O-poor condition, this defect has very high formation energy. In the O-rich limit, the Ga vacancy is stable in the 3$-$ charge state, V_{Ga}^{3-}, acting as a compensation center to n-type conductivity.

3. Antisites

As mentioned before, the antisites, especially Zn$_{Ga}$ and Ga$_{Zn}$, play an important role in the electronic conductivity of ZnGa$_2$O$_4$. While Ga$_{Zn}$ is the lowest-energy donor defect and a likely source of unintentional n-type conductivity, Zn$_{Ga}$ is the lowest-energy acceptor defect that acts as an electron compensation center.

With the antisites, we can define the Fermi level pinning for n- and p-type conductivity (E_{pin}^n and E_{pin}^p, respectively) as the maximum and minimum position for E_F in the system, taking the VBM as a reference [36–39]. From another perspective, the Fermi level pinning determines the condition before the intrinsic defect starts to compensate the prevalent conductivity in the material [36–39]. For materials that are easy to dope n-type, E_{pin}^n lies near the edge or resonant in the conduction
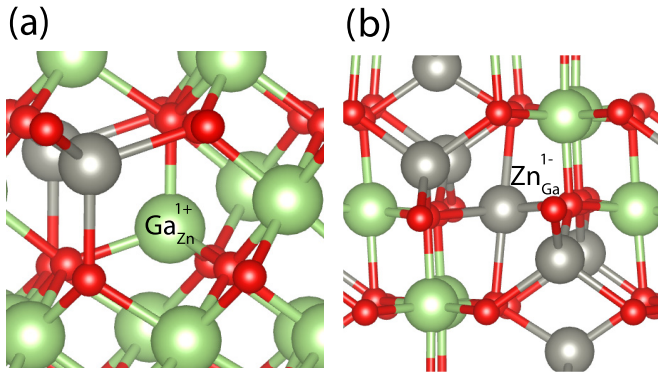
FIG. 5. Local chemical environment for antisite defects (a) gallium substitutional on zinc site in a 1+ charge state and (b) zinc substitutional on a gallium site in a 1− charge state. The oxygen, zinc, and gallium atoms are represented by the red, gray, and green colors, respectively.

band, while for materials that are easily doped p-type, E_{pin}^p lies in the vicinity of the VBM or below it. If the Fermi level pinning for electrons (holes) lies in the middle of a wide band gap, the material tends to not be doped n-type (p-type). If both E_{pin}^n and E_{pin}^p lie in the middle of a wide band gap, the material tends to show insulating behavior for any condition of chemical potential. It is important to emphasize that the pinning of the Fermi level is not necessarily equal to the equilibrium Fermi level. The Fermi level pinning and each antisite defect will be discussed below in detail; the local lattice relaxations associated with Zn_{Ga} and Ga_{Zn} are shown in Fig. 5 and the remaining antisites, with less importance for this material, are shown in Fig. S2 in the Supplemental Material [26].

Gallium on zinc site. In the case of Ga_{Zn}, Ga with a 3+ formal oxidation state replaces Zn with a 2+ formal oxidation state in the tetrahedral sites (8a in the Wyckoff notation). This aliovalent substitution creates one unpaired electron that is weakly bound to Ga. The neutral charge state of Ga_{Zn}^0 is unstable for all values of the Fermi level when compared to the ionized Ga_{Zn}^{1+}, and therefore Ga_{Zn} is considered to be a shallow donor. In the tetrahedral chemical environment of Ga_{Zn}^{1+}, shown in Fig. 5(a), the Ga_{Zn}-O bond length is 1.88 Å, i.e., 2.59% smaller than the original Zn-O bond length of 1.93 Å.

Among all the intrinsic donor defects, the formation energy of Ga_{Zn}^{1+} is the lowest in both O-rich and O-poor conditions. These results have two consequences: (i) if $ZnGa_2O_4$ exhibits unintentional n-type conductivity or is a semi-insulator, the main source of electrons in the conduction band or hole compensation is Ga_{Zn}; (ii) the low formation energy of this defect indicates that Ga can incorporate in the tetrahedral sites in large concentrations, as observed in recent experiments [3–5].

The formation energy of Ga_{Zn} also determines E_{pin}^p, which is given by the point where the formation energy of Ga_{Zn}^{1+} is equal to zero in the O-rich condition with the richest Zn chemical potential, which is not exactly the A point used to plot Fig. 3. If the Fermi level moves from E_{pin}^p towards the VBM, Ga_{Zn} will have negative formation energy, and it will form spontaneously. Under this condition, holes will be automatically compensated by the electrons from Ga_{Zn}.

Therefore, Fermi level pinning at ∼2 eV above the VBM and the high stability of the small hole polaron makes it very difficult to realize p-type conductivity in $ZnGa_2O_4$.

Zinc on gallium site. In this case, Zn substitutes on the octahedral Ga site (16d in Wyckoff notation). In the neutral charge state, Zn_{Ga} leaves an unpaired electron in the valence band that becomes a localized hole in the form of a small polaron sitting on a neighboring O atom. More precisely, the hole is derived from hybridization of Zn $d_{x^2-y^2}$ with O p orbitals, as shown in Fig. S3 in the Supplemental Material [26], and differs from the polaron previously discussed and shown in Fig. 4(a). The hole localization, in this case, is accompanied by a local lattice relaxation in which the Zn_{Ga}-O bond length is shorter (4.3%) than the original Ga-O bond length. By adding one electron to form Zn_{Ga}^{1-}, the hole polaron vanishes and the octahedral environment Zn_{Ga}, shown in Fig. 5(b), becomes more symmetric. The Zn_{Ga}-O bond length of 2.10 Å is 3.96% longer than the original Ga-O bond length of 2.02 Å.

As shown in Fig. 3, neutral Zn_{Ga}^0 is stable only for E_F near the VBM. However, its formation energy is high in both O-rich and O-poor conditions. The negative charge state, Zn_{Ga}^{1-}, is stable for E_F larger than 1.15 eV, marking the (0/−) thermodynamic transition level. Zn_{Ga}^{1-} has the lowest formation energy among all the acceptor intrinsic defects in the O-poor condition and is comparable to V_{Zn}^{2-} and V_{Ga}^{3-} in the O-rich condition for E_F near the CBM. Therefore, we predict that Zn_{Ga} is one of the main sources of electron compensation in $ZnGa_2O_4$, determining E_{pin}^n. The pinning Fermi level for the electrons is calculated at the point where Zn_{Ga}^{1-} has its formation energy equal to zero in the O-poor with Ga-richest chemical potential condition (which is not exactly the point B used to plot Fig. 3), and it lies 0.23 eV above the CBM (inside the conduction band). In other words, for $E_F > E_{pin}^n$, electrons added to the material will fill the holes associated with Zn_{Ga}. Having E_{pin}^n near the CBM indicates that $ZnGa_2O_4$ can be easily doped n-type, and that if doped with impurities, high electron concentrations can eventually be attained, even compared to Ga_2O_3, as reported by recent experiments [4].

Cations on oxygen site. The substitution of O for Zn or Ga (Zn_O, Ga_O) in the tetrahedral environment (32e in Wyckoff notation) creates an excess of electrons and a large Coulomb repulsion between the atoms around it. This repulsion is so strong that it repels one Zn atom from the original lattice in the tetrahedral (8a) to the interstitial site (16c); the neighboring Zn atom relaxes from a tetrahedral motif to an octahedral environment, as shown in Fig. S2 in the Supplemental Material [26]. The displacement of the Zn atom is needed to accommodate the much larger Zn_O or Ga_O atoms, compared to the size of the original O atom.

In the formation energy plot shown in Fig. 3, Zn in the O site is stable in the 2+ charge, Zn_O^{2+}. On the other hand, Ga_O is stable in three charge states, 3+, 1+, and 0, with transitions (3+/1+) 0.64 eV and (1+/0) 0.24 eV below the CBM. If we consider E_F near the CBM (n-type conductivity), all of these defects have very high formation energy, regardless of the O chemical potential. This indicates that Zn_O and Ga_O cannot be a possible source of electrons in n-type $ZnGa_2O_4$. The formation energy of Zn_O and Ga_O is low or negative only for E_F below the middle of the band gap. However, as

noted before, E_{pin}^{p} does not allow E_F to go to this region, and therefore, in general, we can conclude that the concentration of cations in the O site would be negligible in $ZnGa_2O_4$.

Oxygen on cation site. We tested the possibility of O substituting on Zn and Ga sites, namely, O_{Zn} and O_{Ga}, in $ZnGa_2O_4$. In the relaxed configuration, O_{Ga} binds with a neighboring O atom, forming a O_{Ga}-O split interstitial, with a bond length of 1.34 Å, as shown in Fig. S2 in the Supplemental Material [26]. For O_{Zn}, the O_{Zn}-O bond length is 1.41 Å. However, in this configuration, both O atoms bond to two Ga neighbors, likely due to the small internal volume of the $8a$ tetrahedral compared to the $16d$ octahedral.

As seen in Fig. 3, O_{Zn} and O_{Ga} can act as donors or acceptors. If E_F lies close to the VBM (CBM), the most stable charge defect is the $2+$ ($2-$), being amphoteric. Note that the neutral charge state is not stable for both defects, and a negative-U behavior is observed with a transition from $1-$ to $1+$ at 2.07 and 1.95 eV above the VBM for O_{Zn} and O_{Ga}, respectively. Similar to the cation on the O site, the formation energies of O_{Zn} and O_{Ga} are very high in the possible range of E_F determined by E_{pin}^{n} and E_{pin}^{p}. As a consequence, we do not expect large concentrations of O_{Zn} and O_{Ga} in $ZnGa_2O_4$.

4. Interstitials

There are two nonequivalent interstitial sites in the spinel crystal structure, labeled $16c$ and $8b$ according to the Wyckoff notation. Both are shown in Fig. S1 in the Supplemental Material [26]. The $16c$ interstitial site is surrounded by six equidistant O atoms at 2.16 Å, forming an octahedral motif. The $8b$ site is surrounded by four equidistant O at 1.67 Å and four Ga at 1.81 Å. We tested both the $16c$ and $8b$ sites for Zn, Ga, and O; the formation energies are shown in Fig. 3. Because of the small volume of the $8b$ site, it is unlikely that Zn or Ga will occupy this interstitial site, leading to formation energies that are significantly higher than Zn or Ga occupying the $16c$ site. The local lattice relaxation associated with the interstitial defects, for the most stable charge states, is shown in Fig. S2 in the Supplemental Material [26].

Cations interstitial. As noted, the most stable interstitial site for Ga_i and Zn_i is the $16c$. In both cases, the interstitial cation is arranged in an octahedral environment with Ga-O bond length that ranges from 1.94 to 2.04 Å, while for Zn-O, it ranges from 2.10 to 2.11 Å. In addition, Ga_i and Zn_i disturb the local chemical environment of the first Zn neighbors, moving them outward from the interstitial. This repulsion is stronger for Ga_i and is observed in the local atomic environment shown in Fig. S2 in the Supplemental Material [26]. The ionized defect composes the most stable configuration. In the case of Zn (Ga), two electrons of an s orbital (2 from s and 1 from p) are weakly bound, so that these interstitials are most stable in the $2+$ ($3+$) charge states, acting as donors.

In Fig. 3, for both O-rich and O-poor conditions, Ga_i and Zn_i have very high formation energies when E_F is near the CBM; therefore, we do not expect that these defects contribute to the observed unintentional n-type conductivity. Only in the region with E_F below the middle of the band gap do Ga_i and Zn_i have low formation energies, being a potential source of hole compensation in $ZnGa_2O_4$. This behavior is very similar

to the cation on the O site, especially in O-poor conditions, where their formation energies are very similar.

Oxygen interstitial. We tested the O interstitial in both $16c$ and $8b$ Wyckoff positions. For O_i in the $8b$ position, we observed a special condition that we call O_{split}, i.e., the interstitial O binds to a native O, forming an O-O with a bond length of 1.41 Å, suggesting a formation of an O_2 molecule. This configuration is shown in Fig. S2 in the Supplemental Material [26]. The antibonding π^* of O_{split} lies in the band gap of $ZnGa_2O_4$ and is completely occupied in the neutral charge state. A situation similar to that is observed in In_2O_3 and ZnO [10,11]. Due to the occupation of π^*, the bond length of the O_2 molecule in $ZnGa_2O_4$ is larger than the isolated O_2 one, and similar to the O_2^{2-} configuration. It is important to note that O_{split} is stable only in the neutral charge state and has high formation energy. Therefore, even if O_{split} is formed in $ZnGa_2O_4$, this defect will not contribute for n- or p-type conductivity.

The second configuration for O interstitial in the $16c$ site, O_i, has a linear bond with two Zn atoms, forming a Zn-O-Zn structure with an angle of $179°$. This configuration is stable in two charge states: neutral and $1-$, with a transition level of 2.53 eV below the CBM. However, similar to O_{split}, the formation energy of O_i is very high, and we do not expect a large concentration of this defect even in the O-rich condition. This is a good point for a n-type conductivity because O_i acts as a source of electron compensation in $ZnGa_2O_4$.

C. Source of p-type conductivity

According to our calculations, intrinsic p-type conductivity is unlikely in $ZnGa_2O_4$ for three reasons: (i) The holes tend to localize in the form of small polarons due to the localized character of the valence band. These polarons are very stable. (ii) There are no intrinsic shallow acceptors with small formation energy in the vicinity of the valence band, which creates a problem for holes generation. (iii) The Fermi level pinning for the p-type, E_{pin}^{p}, lies around 2 eV above the VBM, and therefore the Fermi level cannot be moved towards the VB without hole compensation by intrinsic donor defects. Despite all these points, experimental results indicate a possible low p-type conductivity in high temperature, under O-rich conditions, with a hole density that does not exceed 10^{15} cm^{-3} [3–5].

To investigate this condition, we suppose an alloy of $ZnGa_2O_4$ with an excess of Zn, forming $Zn_{(1+2x)}Ga_{2(1-x)}O_4$. These extra Zn atoms occupy the Ga site, forming Zn_{Ga}. The calculations were performed for a concentration $x = 0.25$, i.e., an increase of 25% of the Zn atoms in the system. This concentration corresponds to the minimum value that could be added to the primitive spinel structure. For a smaller Zn concentration, a larger unit cell is required and the results are conceptually similar to those using the primitive spinel cell.

The excess of Zn atoms creates an intermediate band that is semi-occupied, assuming all Zn_{Ga} are in the neutral charge state. However, just to determine the characteristic of the intermediate band by the analysis of the density of states, we suppose a completely unoccupied band (to avoid nonrealistic spin polarization in the alloy) with the Fermi energy at the top of the host O $2p$ band. The detached band is composed
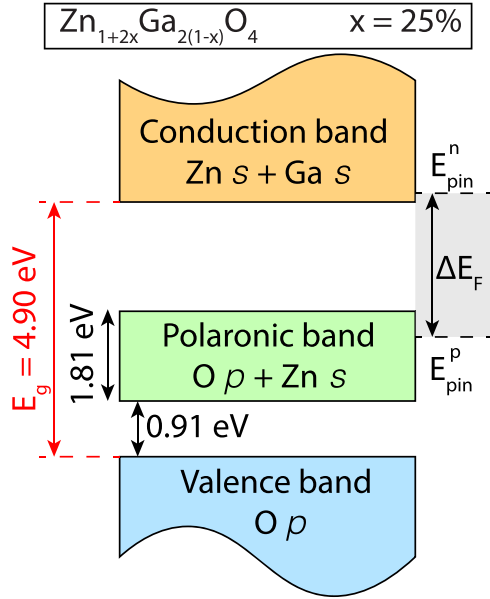
FIG. 6. Schematic bands diagram for $Zn_{(1+2x)}Ga_{2(1-x)}O_4$ alloy with $x = 0.25$. The detached band, shown in green, is called the polaronic band and is composed of hybridization of O 2p and Zn 3d orbitals. The maximum and minimum variation of the Fermi level is shown in the gray area on the right side, with the pinning for p-type conductivity, E_{pin}^p, crossing the polaronic band.

of the hybridization of O 2p orbitals and Zn 3d orbitals (orbitals of the extra Zn in the system), forming a charge distribution similar to the polaron discussed previously in the point defect Zn_{Ga} and shown in Fig. S3 of the Supplemental Material [26]. The calculated density of states of this system is shown in Fig. S4 of the Supplemental Material [26]. Therefore, we assign a polaronic nature to the detached band. The formation of a detached band is observed in other alloys of oxides, such as In_2O_3 and Ga_2O_3 with dilute concentrations of Bi [40,41]. Also, intermediate bands play an important role in antidoping processes in quantum materials [42] and have also been proposed for the construction of high-efficiency solar cells [43,44].

As we can observe in Fig. 6, the polaronic band lies at ~0.9 eV above the host valence-band maximum and has a width of 1.8 eV. The pinning of the Fermi level for p-type conductivity, E_{pin}^p, lies inside this band. The possible Fermi level variation is shown in the gray area on the right side of Fig. 6. This means that it is possible to shift down the Fermi level to create holes in the polaronic band before the intrinsic donor defects Ga_{Zn} start to form spontaneously and start to compensate the holes. In other words, it is possible to have a p-type conductivity inside the polaronic band. Despite that, the conductivity should occur by hopping of the localized hole in O and Zn atoms, which can lead to low charge mobility. It is important to mention that the addition of 25% of Zn is not a necessary condition to obtain the polaronic band. Smaller concentrations of Zn in the alloy $Zn_{(1+2x)}Ga_{2(1-x)}O_4$ decrease the width of the polaronic band because of the weaker interaction between the extra Zn [40,41], but the intermediate band is still present. Thus, the width and the nature of the detached band in $ZnGa_2O_4$, grown under O-rich conditions, explain the low

hole mobility and the required high temperature to observe the p-type conductivity. Therefore, we can say that the p-type conductivity occurs in the detached polaronic band formed by an excess of Zn atoms in the system and does not occur in the valence band as suggested previously [3,4].

D. Optical emission

In the optical measurement, the peaks in the photoluminescence spectrum could be a fingerprint of the defects states in the material. Considering that, we calculate the emission photon energy for the most stable defects in $ZnGa_2O_4$: hole polaron, V_O, V_{Ga}, V_{Zn}, and Zn_{Ga}. It is important to mention that the emission spectrum was calculated according to the Franck-Condon approximation in the generalized coordination diagram, a procedure applied before for other oxides [10,45]. According to the Fermi level pinning, E_{pin}^n and E_{pin}^p, $ZnGa_2O_4$ can have the Fermi level between the middle of the band gap and the CBM, and we considered that range to calculate the optical emission spectrum for defects. In this range, only V_O has two charge states with high stability: 2+ and 0, and therefore we considered both charge configurations. For all the remaining defects, V_{Ga}, V_{Zn}, and Zn_{Ga}, we considered only the most stable charge state. This methodology to compute the emission spectrum for defects does not have a high precision if the defects have a shallow donor or acceptor characteristic. Therefore, we removed the antisite Ga_{Zn} from our discussion.

For photons with energy larger than the band gap, electrons from the valence band are promoted to the conduction band, leaving holes behind. Because of the high stability of the small hole polaron in $ZnGa_2O_4$, the atoms around one O relax to localize the hole, resulting in a quasiparticle state inside the band gap. After atomic relaxation, a free electron in the conduction band will be attracted to the small polaron and recombine, emitting light. In $ZnGa_2O_4$, this recombination emits a photon with an energy of 3.18 eV (at the peak) which corresponds to the edge of the visible spectrum, close to the ultraviolet region. This recombination process is shown in Fig. 7. The absorption, emission, and zero phonon lines in the generalized coordinate diagram are shown in the Supplemental Material (Fig. S5) [26] for all the defects.

For V_O, two processes can occur according to the Fermi level position. First, if E_F is deeper and lies in a region where V_O^{2+} is the most stable charge state, the incidence of a photon can excite one electron from the valence band to the quasiparticle level of V_O^{2+} that lies in resonance in the conduction band, as discussed before. This procedure changes the charge state from V_O^{2+} to V_O^{1+} according to the reaction: $V_O^{2+} + 1e + 1h \rightarrow V_O^{1+} + 1h$. After the atomic relaxation around the oxygen vacancy, V_O^{1+} becomes unstable and tends to return to the V_O^{2+} configuration by a recombination with the extra hole in the system, resulting in two possible routes. In the first route, we assume that there is not sufficient time for a hole relaxation and therefore there is no polaron formation. Thus, V_O^{1+} will recombine with a hole in the valence band, emitting a photon with energy equal to 2.47 eV, which lies in the visible spectrum and corresponds to the green color. In the second route, a hole polaron forms and V_O^{1+} will
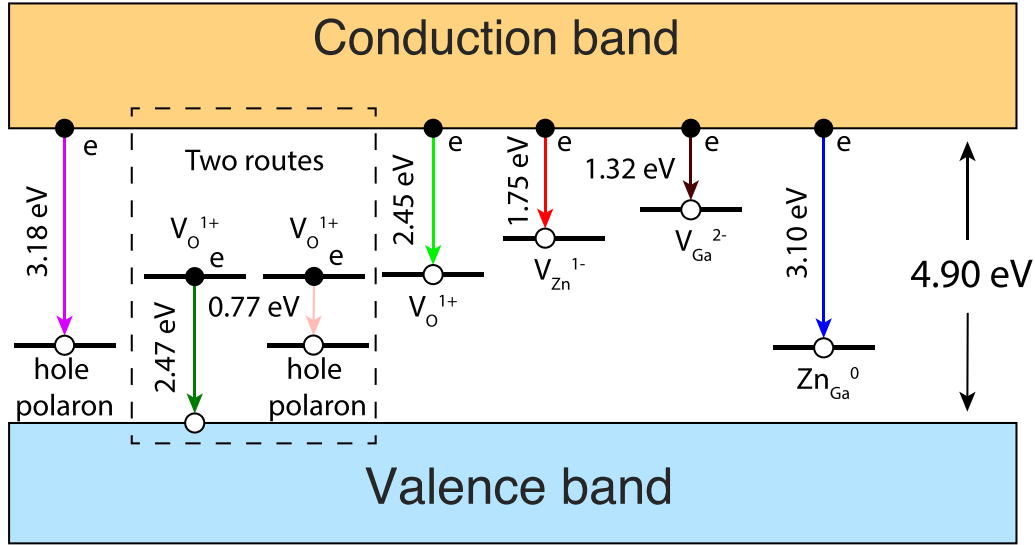
FIG. 7. Optical emission of the most stable intrinsic defects of $ZnGa_2O_4$ calculated according to the Franck-Condon effect in the generalized coordination diagram. The filled (open) circle represents the electron (hole).

recombine with the hole polaron, emitting a photon with energy equal to 0.77 eV, which corresponds to the infrared spectrum.

The second procedure that can occur with V_O is when the E_F is closer to the CBM. Under this configuration, the neutral oxygen vacancy is the most stable one, V_O^0. The incidence of photons in the material can promote one electron of V_O^0 to the conduction band, and promote the reaction: $V_O^0 + 1h + 1e \rightarrow V_O^{1+} + 1e$. Again, the V_O^{1+} configuration is not stable and there is a tendency to capture one electron and return to the neutral charge state (in this condition, the electron does not form a polaron and there is only one route of recombination). This procedure leads to a photon emission with an energy of 2.45 eV, which is very similar to the first route of the previous condition. Therefore, we expect that the emissions associated with V_O occur in the green color, or infrared, with both conditions shown in Fig. 7. The green emission is observed by experimentalists with photon energy around 2.48 eV (499 nm) [46].

Considering the other two vacancies, V_{Zn} and V_{Ga}, the procedure is very similar to the second condition of V_O. A photon promotes one electron that lies in the defect state of V_{Zn}^{2-} (V_{Ga}^{3-}) to the conduction band, resulting in the reaction: V_{Zn}^{2-} (V_{Ga}^{3-}) $+ 1h + 1e \rightarrow V_{Zn}^{1-}$ (V_{Ga}^{2-}) $+ 1e$. The excited state tends to return to the ground state and recombine with a free electron from the conduction band. This procedure emits a photon with energy equal to 1.75 eV for V_{Zn} and 1.32 eV for V_{Ga}, which correspond to a spectrum with red color and at the infrared region, respectively.

Considering the antisite Zn_{Ga}, the incident light in $ZnGa_2O_4$ promotes one electron from the Zn_{Ga}^{1-} state to the conduction band by the process: $Zn_{Ga}^{1-} + 1h + 1e \rightarrow Zn_{Ga}^0 + 1e$. If the Fermi level is close to the CBM, Zn_{Ga}^0 is unstable and tends to capture one free electron to return to the original charge state. A photon with energy equal to 3.10 eV, which is close to the UV spectrum, is emitted in this procedure. According to the emission spectrum fingerprint,

we can say that it is hard to distinguish the hole polaron and Zn_{Ga} defect.

IV. SUMMARY AND CONCLUSIONS

In summary, we calculate the electronic, optical, and defect properties in $ZnGa_2O_4$, a potential candidate for high-energy power electronics and UV detectors. We observe that antisites play an important role in the conductivity of $ZnGa_2O_4$. While Ga_{Zn} is likely the main source of unintentional n-type conductivity, Zn_{Ga} is the most stable acceptor defect and the main source of electron compensation. The p-type conductivity in the valence band is difficult to achieve. There is a large tendency for hole localization in the form of small polarons, either as self-trapped holes or bound to intrinsic defects, pinning the Fermi level far above the VBM.

We conclude that p-type conductivity in $ZnGa_2O_4$ could be achieved only with excess Zn atoms. This will form an intermediate polaronic band inside the band gap of the material. In this band, the conductivity occurs by hopping, which explains the low mobility and low hole density observed in experimental results. In addition, we compute the emission spectrum of the lowest-energy defects in $ZnGa_2O_4$. Most of the defects that are associated with polarons emit in the spectrum close to ultraviolet, while the oxygen vacancy can emit in the green or infrared. The possibility for both types of conductivity, better thermal dissipation, and isotropic properties make $ZnGa_2O_4$ a potential candidate to replace Ga_2O_3, or at least complement it as an ultrawide band-gap material for electronic and optoelectronic applications.

---

[1] J. Y. Tsao, S. Chowdhury, M. A. Hollis, D. Jena, N. M. Johnson, K. A. Jones, R. J. Kaplar, S. Rajan, C. G. Van de Walle, E. Bellotti, C. L. Chua, R. Collazo, M. E. Coltrin, J. A. Cooper, K. R. Evans, S. Graham, T. A. Grotjohn, E. R. Heller, M. Higashiwaki, M. S. Islam *et al.*, Adv. Electron. Mater. **4**, 1600501 (2018).

[2] P. Gorai, R. W. McKinney, N. M. Haegel, A. Zakutayev, and V. Stevanovic, Energy Environ. Sci. **12**, 3338 (2019).

[3] M.-I. Chen, A. K. Singh, J.-L. Chiang, R.-H. Horng, and D.-S. Wuu, Nanomaterials **10**, 2208 (2020).

[4] E. Chikoidze, C. Sartel, I. Madaci, H. Mohamed, C. Vilar, B. Ballesteros, F. Belarre, E. del Corro, P. Vales-Castro, G. Sauthier, L. Li, M. Jennings, V. Sallet, Y. Dumont, and A. Pérez-Tomás, Cryst. Growth Des. **20**, 2535 (2020).

[5] Z. Chi, F.-G. Tarntair, M. Frégnaux, W.-Y. Wu, C. Sartel, I. Madaci, P. Chapon, V. Sallet, Y. Dumont, A. Pérez-Tomás, R. Horng, and E. Chikoidze, Mater. Today Phys. **20**, 100466 (2021).

[6] S. J. Pearton, J. Yang, P. H. Cary IV, F. Ren, J. Kim, M. J. Tadjer, and M. A. Mastro, Appl. Phys. Rev. **5**, 011301 (2018).

[7] M. A. Mastro, A. Kuramata, J. Calkins, J. Kim, F. Ren, and S. J. Pearton, ECS J. Solid State Sci. Technol. **6**, P356 (2017).

[8] Z. Galazka, S. Ganschow, R. Schewski, K. Irmscher, D. Klimm, A. Kwasniewski, M. Pietsch, A. Fiedler, I. Schulze-Jonack, M. Albrecht, T. Schröder, and M. Bickermann, APL Mater. **7**, 022512 (2019).

[9] N. Ma, N. Tanen, A. Verma, Z. Guo, T. Luo, H. G. Xing, and D. Jena, Appl. Phys. Lett. **109**, 212101 (2016).

[10] I. Chatratin, F. P. Sabino, P. Reunchan, S. Limpijumnong, J. B. Varley, C. G. Van de Walle, and A. Janotti, Phys. Rev. Mater. **3**, 074604 (2019).

[11] A. Janotti and C. G. Van de Walle, Phys. Rev. B **76**, 165202 (2007).

[12] J. B. Varley, J. R. Weber, A. Janotti, and C. G. V. de Walle, Appl. Phys. Lett. **97**, 142106 (2010).

[13] M. Buonanno, D. Welch, I. Shuryak, and D. J. Brenner, Sci. Rep. **10**, 10285 (2020).

[14] H. Dixit, N. Tandon, S. Cottenier, R. Saniz, D. Lamoen, B. Partoens, V. V. Speybroeck, and M. Waroquier, New J. Phys. **13**, 063002 (2011).

[15] Y. Xia, T. Wang, X. Zhao, X. Jiao, and D. Chen, J. Phys. Chem. C **122**, 5509 (2018).

[16] J. L. Lyons, J. Appl. Phys. **131**, 025701 (2022).

[17] P. Hohenberg and W. Kohn, Phys. Rev. **136**, B864 (1964).

[18] W. Kohn and L. J. Sham, Phys. Rev. **140**, A1133 (1965).

[19] J. Heyd and G. E. Scuseria, J. Chem. Phys. **120**, 7274 (2004).

[20] J. Heyd, G. E. Scuseria, and M. Ernzerhof, J. Chem. Phys. **124**, 219906 (2006).

[21] G. Kresse and J. Hafner, Phys. Rev. B **48**, 13115 (1993).

[22] G. Kresse and J. Furthmüller, Phys. Rev. B **54**, 11169 (1996).

[23] P. E. Blöchl, Phys. Rev. B **50**, 17953 (1994).

[24] G. Kresse and D. Joubert, Phys. Rev. B **59**, 1758 (1999).

[25] C. G. Van de Walle and J. Neugebauer, J. Appl. Phys. **95**, 3851 (2004).

[26] See Supplemental Material at http://link.aps.org/supplemental/10.1103/PhysRevMaterials.6.064602 for structural and defects local chemical environments, alloy electronic structure and convergence tests.

[27] C. Freysoldt, J. Neugebauer, and C. G. Van de Walle, Phys. Rev. Lett. **102**, 016402 (2009).

[28] C. Freysoldt, J. Neugebauer, and C. G. Van de Walle, Phys. Status Solidi B **248**, 1067 (2011).

[29] C. Freysoldt, B. Grabowski, T. Hickel, J. Neugebauer, G. Kresse, A. Janotti, and C. G. Van de Walle, Rev. Mod. Phys. **86**, 253 (2014).

[30] A. Alkauskas, M. D. McCluskey, and C. G. Van de Walle, J. Appl. Phys. **119**, 181101 (2016).

[31] C. Zimmermann, Y. K. Frodason, A. W. Barnard, J. B. Varley, K. Irmscher, Z. Galazka, A. Karjalainen, W. E. Meyer, F. D. Auret, and L. Vines, Appl. Phys. Lett. **116**, 072101 (2020).

[32] F. P. Sabino, L. N. de Oliveira, and J. L. F. Da Silva, Phys. Rev. B **90**, 155206 (2014).

[33] F. P. Sabino, R. Besse, L. N. Oliveira, S.-H. Wei, and J. L. F. Da Silva, Phys. Rev. B **92**, 205308 (2015).

[34] J. B. Varley, A. Janotti, C. Franchini, and C. G. Van de Walle, Phys. Rev. B **85**, 081109(R) (2012).

[35] T. Gake, Y. Kumagai, and F. Oba, Phys. Rev. Mater. **3**, 044603 (2019).

[36] S. B. Zhang, S.-H. Wei, and A. Zunger, Phys. Rev. Lett. **84**, 1232 (2000).

[37] A. Zunger, Appl. Phys. Lett. **83**, 57 (2003).

[38] S.-H. Wei, Comput. Mater. Sci. **30**, 337 (2004).

[39] F. P. Sabino, A. Zunger, and G. M. Dalpian, Mater. Horiz. **9**, 791 (2022).

[40] F. P. Sabino, S.-H. Wei, and A. Janotti, Phys. Rev. Mater. **3**, 034605 (2019).

[41] X. Cai, F. P. Sabino, A. Janotti, and S.-H. Wei, Phys. Rev. B **103**, 115205 (2021).

[42] Q. Liu, G. M. Dalpian, and A. Zunger, Phys. Rev. Lett. **122**, 106403 (2019).

[43] A. Luque and A. Martí, Phys. Rev. Lett. **78**, 5014 (1997).

[44] D. J. Baquião and G. M. Dalpian, Comput. Mater. Sci. **158**, 382 (2019).

[45] A. Janotti, J. B. Varley, M. Choi, and C. G. Van de Walle, Phys. Rev. B **90**, 085202 (2014).

[46] R.-H. Horng, C.-Y. Huang, S.-L. Ou, T.-K. Juang, and P.-L. Liu, Cryst. Growth Des. **17**, 6071 (2017).